Journal of Solid State Chemistry 182 (2009) 2202–2207

Contents lists available at ScienceDirect

Journal of Solid State Chemistry

journal homepage: www.elsevier.com/locate/jssc

Hydrothermal synthesis and characterization of two new layered vanadium tellurites Cu(TATP)V_2TeO_8 and Cu(DPPZ)$V_2Te_2O_{10}$

Guang-Xi Han, Yong-Juan Song, Zheng-Bo Han *

College of Chemistry, Liaoning University, Shenyang 110036, PR China

ARTICLE INFO

Article history:
Received 31 March 2009
Received in revised form
13 May 2009
Accepted 27 May 2009
Available online 2 June 2009

Keywords:
Vanadium tellurites
Hydrothermal synthesis
V–Te–O
Helical chain

ABSTRACT

Two new vanadium tellurites, Cu(TATP)V_2TeO_8 **(1)** and Cu(DPPZ)$V_2Te_2O_{10}$ **(2)**, (TATP = 1,4,8,9-tetranitrogen-trisphene, DPPZ = dipyridophenazine) have been synthesized under hydrothermal conditions and structurally characterized by elemental analyses, IR, and single-crystal X-ray diffraction. Compound **1** features an interesting two-dimensional layer structure constructed by $[V_2TeO_8]_n$ double-chain-like ribbons linked by $[Cu(TATP)]^{2+}$ bridges. Compound **2** consists of two types of chiral layers: one left-handed and the other right-handed, which lead to racemic solid-state compound. In each layer, there exist two types of inorganic helical chains $(V_4Te_4O_8)_n$ and $(Te_2O_2)_n$, with same handedness. Two types of helical chains are linked by μ_3(O6) atoms to generate a V/Te/O inorganic anionic layer. The $[Cu(DPPZ)]^{2+}$ cationic complex fragments are covalently bonded to the layer, projecting below and above the vanadium tellurites layer.

1. Introduction

There has been extensive interest in inorganic–organic hybrid materials not only because of their remarkable compositional range and structural diversity but also owing to their potential applications in the fields of catalysis, biology, optics and electromagnetic functional materials [1,2]. One remarkable feature of the hybrid materials is that the organic components act as ligands directly coordinated to the inorganic scaffoldings or to the secondary metal atoms, which can lead to not only the functionality of inorganic–organic hybrids being multiplied by the incorporation of organic and inorganic counterparts into one structural unit, but also these hybrid materials manifesting the structural influences both of the coordination preferences of the secondary metal site and of the geometric constraints of the ligand [3–7]. An important advance in this field is the design of organic–inorganic hybrid vanadium oxide materials in which vanadium oxides are templated or coordinated by transition-metal complexes or fragments. Up to now, a serial of organic–inorganic hybrid materials have been synthesized, which exhibit interesting discrete cluster, one-dimensional (1D) chain, layer structure, and three-dimensional (3D) structure. Most of them belong to the {M_xL_y/V/O}, {M_xL_y/V/P/O}, {M_xL_y/Mo/O}, and {M_xL_y/Mo/P/O} systems (M = transition metal, L = organic ligand) [8–12]. Compared with the systems mentioned above, {M_xL_y/V/Te/O} system is rarely documented [13].

The prediction of coordination frameworks is still subjective and cannot be generalized because the self-assembly progress is highly influenced by several factors, such as the metal/ligand nature [14], solvent [15], templates [16], counter ions [17]. In this respect, the influence of ligand spacers of flexible bridging ligands on framework formation of their coordination polymers have widely been documented [18]. However, the studies on the effect of the size of N-donor chelate ligand on framework formation of their complexes have rarely been reported [19]. In this paper, we report two new vanadium tellurites with an N-donor chelate ligand 1,4,8,9-tetranitrogen-trisphene (TATP) and its large analog dipyridophenazine (DPPZ) and studied the influences of the size of the aromatic chelate ligands on the framework structures, namely Cu(TATP)V_2TeO_8 **(1)** and Cu(DPPZ)$V_2Te_2O_{10}$ **(2)**.

2. Experimental

2.1. Materials and methods

The aromatic chelate ligands TATP and DPPZ were synthesized according to the literature method [20]; all other reagents and solvents employed were commercially available and used as received without further purification. The C, H, and N micro-analyses were carried out with Perkin-Elmer 240 elemental analyzer. The FT–IR spectra were recorded from KBr pellets in the 4000–400 cm^{-1} range on a Nicolet 5DX spectrometer.

* Corresponding author. Fax: +86 24 62202380.
E-mail address: ceshzb@lnu.edu.cn (Z.-B. Han).

0022-4596/$ - see front matter Crown Copyright © 2009 Published by Elsevier Inc. All rights reserved.
doi:10.1016/j.jssc.2009.05.038

2.2. Hydrothermal syntheses

Cu(TATP)V_2TeO_8 (**1**): A mixture of V_2O_5 (0.091 g, 0.5 mmol), $CuCl_2$ (0.043 g, 0.3 mmol), TATP (0.116 g, 0.5 mmol), H_2TeO_4 (0.194 g, 1.0 mmol) and H_2O (10 ml) was mixed in a 23 ml Teflon reactor, which was heated at 180 °C for 6 days and then slow cooled to room temperature. Green block crystals of **1** were obtained in 38% yield (based on V) after being washed with distilled water and dried at ambient temperature. Anal. Calcd. for $C_{14}H_8CuN_4O_8TeV_2$ (**1**): C, 25.74; H, 1.23; N, 8.58%. Found: C, 25.86; H, 1.35; N, 8.68%. IR (KBr, cm^{-1}): 1625(m), 1580(m), 1482(w), 1400(s), 1381(w), 1311(m), 1114(m), 1089(m), 1079(w), 999(w), 933(s), 841(m), 788(s), 731(s), 636(m).

Cu(DPPZ)$V_2Te_2O_{10}$ (**2**): The synthesis of **2** was similar to that of **1** except that DPPZ was used in place of TATP. Yield 12% (based on V). Anal. Calcd. for $C_{18}H_{10}CuN_4O_{10}Te_2V_2$ (**2**): C, 25.05; H, 1.17; N, 6.49%. Found: C, 25.35; H, 1.09; N, 6.71%. IR (KBr, cm^{-1}): 3427(s), 2924(m), 1623(s), 1578(s), 1492(w), 1462(s), 1417(w), 1352(m), 1336(m), 1230(m), 1139(m), 1072(m), 990(m), 961(m), 868(m), 817(s), 779(w), 725(s), 678(m), 655(m).

2.3. X-ray crystallography

Crystallographic data of **1** and **2** were collected at room temperature with a Bruker P4 diffractometer with Mo$K\alpha$ radiation ($\lambda = 0.71073$ Å) and graphite monochromator using the ω-scan mode. The structures were solved by direct methods and refined on F^2 by full-matrix least squares using SHELXTL [21]. All non-hydrogen atoms were treated anisotropically. The positions of the hydrogen atoms were generated geometrically. Crystallographic data and experimental details for structural analyses are summarized in Table 1. Selected bond distances and angles are listed in Table 2. The CCDC reference numbers 706723 for **1** and 706724 for **2**. Copy of the data can be obtained free of charge on application to CCDC, 12 Union Road, Cambridge CB2 1EZ, UK (fax: +44 1223 336–033; e-mail: deposit@ccdc.cam.ac.uk).

Table 1
Crystallographic data for **1** and **2**.

	1	**2**
Empirical formula	$C_{14}H_8CuN_4O_8TeV_2$	$C_{18}H_{10}CuN_4O_{10}Te_2V_2$
Formula weight	653.26	862.92
Wavelength (Å)	0.71073	0.71073
Crystal system	Triclinic	Monoclinic
Space group	*P*-1	$P2_1/c$
a (Å)	7.878(2)	8.097(2)
b (Å)	8.030(2)	7.659(2)
c (Å)	14.186(3)	35.248(8)
α (deg)	105.90(2)	90
B (deg)	93.21(2)	96.42(1)
γ (deg)	96.95(2)	90
V (Å^3)	853.0(3)	2172.4(8)
Z	2	4
D_c (g cm^{-3})	2.543	2.638
μ (mm^{-1})	4.043	4.514
F(000)	622	1620
Crystal size (mm)	0.37 × 0.12 × 0.07	0.15 × 0.05 × 0.02
Range for data collection (deg)	2.62–27.50	1.16–26.00
Reflections collected	4036	11889
Independent reflections	3625	4258
Max., min. transmission	0.7706 and 0.3169	0.9072 and 0.5470
T (K)	293(2)	293(2)
Goodness-of-fit on F^2	1.012	1.113
Data/restraints/parameters	3625/0/271	4258/0/334
Final *R* indices [$I>2\sigma(I)$][a]	$R_1 = 0.0364$	$R_1 = 0.0467$
	$wR_2 = 0.0859$	$wR_2 = 0.1055$
R indices (all data)	$R_1 = 0.0515$	$R_1 = 0.0553$
	$wR_2 = 0.1091$	$wR_2 = 0.1099$
Largest diff. peak and hole (*e* Å^{-3})	1.058 and −1.616	1.429 and −1.109

[a] $R_1 = \sum ||F_o| - |F_C|| / \sum |F_o|$; $wR_2 = \sum [w(F_o^2 - F_c^2)^2] / \sum [wF_o^2)^2]^{1/2}$.

Table 2
Selected bond distances (Å) and Angles (°) for **1** and **2**.

1			
Cu(1)–O(4)	1.939(4)	O(4)–Cu(1)–O(2)	95.25(2)
Cu(1)–O(2)	1.949(4)	O(4)–Cu(1)–N(1)	88.83(2)
Cu(1)–N(1)	2.008(5)	N(1)–Cu(1)–N(2)	81.21(2)
Cu(1)–N(2)	2.032(5)	O(2)–Cu(1)–N(2)	97.94(2)
Cu(1)–O(8)♯1	2.211(4)	O(4)–Cu(1)–N(2)	154.8(2)
V(1)–O(5)	1.634(4)	O(5)–V(1)–O(6)	109.9(3)
V(1)–O(4)♯2	1.652(4)	O(5)–V(1)–O(4)♯2	108.0(2)
V(1)–O(6)	1.770(5)	O(4)♯2–V(1)–O(1)	111.1(2)
V(1)–O(1)	1.804(4)	O(7)–V(2)–O(3)	107.8(3)
V(2)–O(7)	1.602(5)	O(8)–V(2)–O(6)♯3	108.1(2)
V(2)–O(8)	1.633(4)	O(7)–V(2)–O(6)♯3	109.9(3)
V(2)–O(3)	1.815(4)	O(7)–V(2)–O(8)	108.2(3)
V(2)–O(6)♯3	1.806(5)	O(1)–Te(1)–O(2)♯4	164.44(2)
Te(1–O(2)	1.872(4)	O(2)–Te(1)–O(3)	93.16(2)
Te(1)–O(3)	1.879(4)	O(2)–Te(1)–O(1)	92.59(2)
Te(1)–O(1)	1.936(4)		
Te(1)–O(2)♯4	2.484(4)		
2			
Cu(1)–N(1)	1.987(5)	N(1)–Cu(1)–O(1)	98.4(2)
Cu(1)–N(2)	2.015(6)	N(1)–Cu(1)–N(2)	82.4(2)
Cu(1)–O(1)	2.390(5)	O(2)–Cu(1)–O(3)	88.57(19)
Cu(1)–O(2)	1.915(5)	O(2)–Cu(1)–O(1)	94.4(2)
Cu(1)–O(3)	1.945(4)	O(5)–V(1)–O(4)	102.6(2)
V(1)–O(5)	1.593(5)	O(5)–V(1)–O(6)	107.7(2)
V(1)–O(3)	1.739(5)	O(3)–V(1)–O(6)	146.2(2)
V(1)–O(8)♯1	1.917(4)	O(3)–V(1)–O(8)♯1	93.4(2)
V(1)–O(4)	1.944(5)	O(5)–V(1)–O(3)	106.2(3)
V(1)–O(6)	1.591(4)	O(1)♯2–V(2)–O(9)	105.2(2)
V(2)–O(1)♯2	1.662(5)	O(1)♯2–V(2)–O(7)♯3	115.3(3)
V(2)–O(7)♯3	1.824(5)	O(10)–V(2)–O(7)♯3	107.7(3)
V(2)–O(9)	1.845(5)	O(6)–Te(1)–O(6)♯4	150.81(8)
V(2)–O(10)	1.609(5)	O(8)–Te(1)–O(6)♯4	68.21(2)
Te(1)–O(6)	1.904(4)	O(8)–Te(1)–O(7)	100.3(2)
Te(1)–O(7)	1.913(4)	O(8)–Te(1)–O(6)	86.39(19)
Te(1)–O(8)	1.888(4)	O(8)–Te(1)–O(7)	100.3(2)
Te(1)–O(6)♯4	2.390(4)	O(6)–Te(1)–O(7)	89.4(2)
Te(1)–O(6)♯4	2.389(5)	O(2)–Te(2)–O(4)	101.5(2)
Te(2)–O(2)	1.846(5)	O(4)–Te(2)–O(9)	94.3(2)
Te(2)–O(9)	1.907(5)	O(2)–Te(2)–O(9)	93.0(2)

Symmetry code for **1**: ♯1 *x*, *y*+1, *z*; ♯2 −*x*, −y+2, −*z*+2; ♯3 *x*+1, y, z; ♯4 −*x*+1, −*y*+2, −*z*+2. For **2**: ♯1 −*x*+3, *y*+1/2, −*z*+1/2; ♯2 *x*, *y*−1, z; ♯3 *x*−1, *y*, *z*; ♯4 −*x*+3, *y*−1/2, −*z*+1/2.

3. Results and discussion

Structure of Cu(TATP)V_2TeO_8 (**1**): The single crystal X-ray analysis suggests that compound 1 is a 2D layer structure constructed from double-chain-like vanadium tellurite ribbons bridged by Cu-TATP complex moieties. There are two crystallographically unique V atoms, one Te atom, one Cu atom, one TATP ligand, and eight oxygen atoms in the asymmetric unit (Fig. 1). Each V atom is four-coordinated by four oxygen atoms in a distorted tetrahedral geometry. The V–O bond lengths are in the range of 1.602(5)–1.815(4) Å, and the O–V–O angles vary from 107.8(3) to 111.8(2). The Cu atom adopts a square-pyramidal geometry, being coordinated by two nitrogen donors of a TATP group, one oxygen atom of the {V(2)O_4} unit, one oxygen atom of the {V(1)O_4} unit and the third oxygen atom of the {TeO_4} unit. In the {TeO_4} unit, one oxygen atom bridges to one V(1), one to V(2) atom and the other two oxygen atoms are linked with two Cu atoms. The Te atom is four-coordinated by four oxygen atoms with the Te–O bond lengths vary from 1.871(4) to 2.484(4) Å, and the

O–Te–O angles are in the range of 73.59(16)–164.44(15)°. The geometry of {TeO_4} can be explained by VSEPR theory as an AX4E trigonal bipyramid, in which the lone pair electrons occupy one equatorial position [22].

The structure of **1** consists of novel double-chain-like vanadium tellurite ribbons, as shown in Fig. 2 and Fig. 1S. It is interesting that the ribbon consist of unusual eight-membered rings {$V_4Te_4O_8$}. Each double-chain contains two single chains which are interconnected by sharing the O(2) atoms and their equivalents. The single chain is constructed by the {V(1)O_4} tetrahedra, {V(2)O_4} tetrahedra and {TeO_4} trigonal pyramid connected in the corner-sharing mode. The adjacent {$V_4Te_4O_8$} double chains are linked together by the $[Cu(TATP)]^{2+}$ complex moieties through sharing oxygen atoms with {VO_4} and {TeO_4} polyhedra from one chain and other {VO_4} from the adjacent chain to from an interesting 2D layer (Fig. 3). In the 2D layer, seven-membered rings {$CuV_3Te_3O_7$} and eight-membered rings {$Cu_2V_4Te_2O_8$} are formed between adjacent double-chain ribbons. Thus, a novel organic–inorganic hybrid layer may be viewed as a network with a 7,8-connected net. The TATP groups project above and below the 2D network. Although the formula of **1** is similar to that of Cu(phen)V_2TeO_8 [13a], its architecture is different from the latter in which the ribbon consists of five-member rings {$V_3Te_2O_5$} and the 2D layer may be viewed as a network with a 3, 5, 6-net.

These layers are further extended into a 3D supramolecular framework through intercalation between the lateral TATP ligands from adjacent layers in a zipperlike, offset fashion with the interplanar distance of *ca.* 3.63 Å (Fig. 4), indicating a moderate $\pi-\pi$ stacking interactions [23]. Furthermore, the interlayers are connected together through hydrogen bonding interactions between the carbon atoms of TATP ligands and oxygen atoms. The typical hydrogen bonds are C12···O3 3.438 (2) Å, C6···O5 ($-x$+1, $-y$, $-z$+1) 3.149 (2) Å [24]. The hydrogen bonding and $\pi-\pi$ stacking interactions enhance the stability of the complex.

Structure of Cu(DPPZ)$V_2Te_2O_{10}$ (**2**): The crystal structure of **2** shows the presence of an unprecedented vanadium tellurite layer covalently grafted by $[Cu(DPPZ)]^{2+}$ fragments. As shown in Fig. 5, there are two crystallographically distinct vanadium atoms in the asymmetric unit. Each V(1) atom is five-coordinated by one terminal oxygen atom and four bridging oxygen atoms, two of which are linked with Te(1) atom, one with Te(2) atom and the fourth with one Cu atom, showing a distorted square pyramid coordination geometry. Each V(2) atom adopts a tetrahedral geometry and is coordinated by a terminal oxygen atom and three

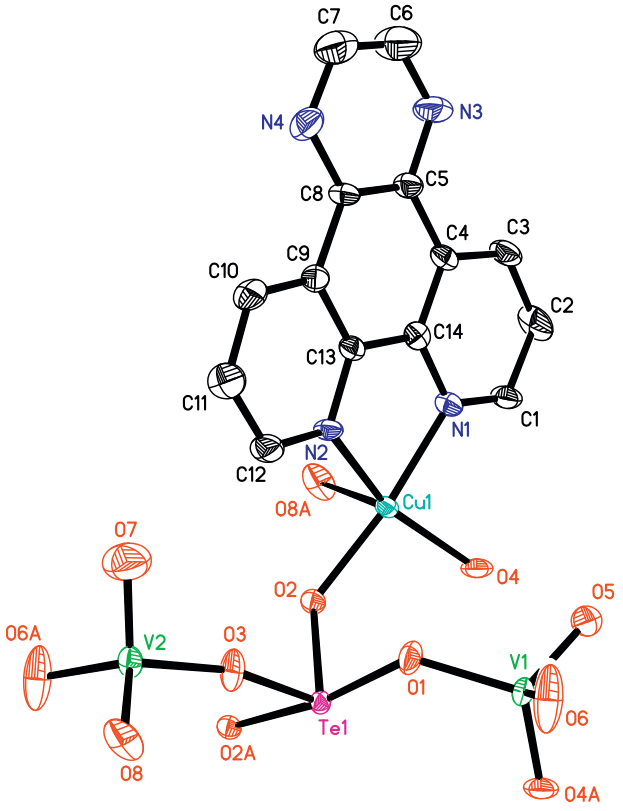

Fig. 1. ORTEP drawing of compound 1 with thermal ellipsoids at 50% probability. H atoms are omitted for clarity.

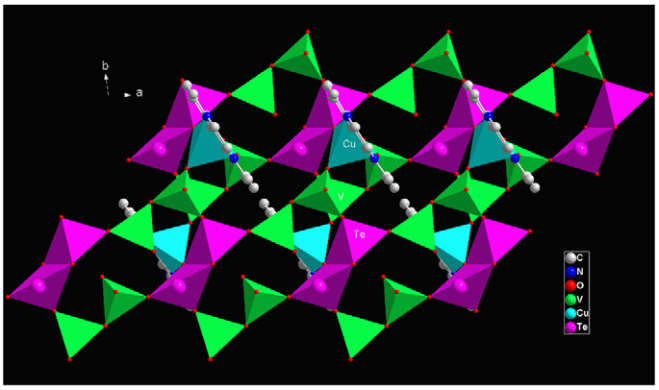

Fig. 3. View of 2D layer of **1** along the *c*-axis.

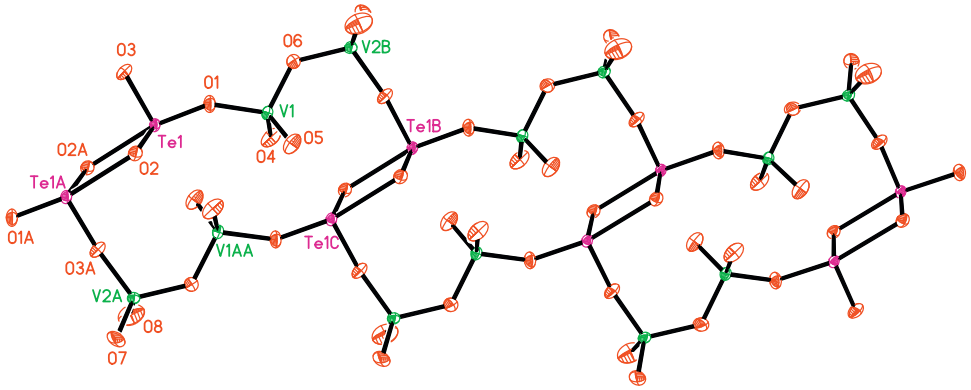

Fig. 2. Double-chain-like ribbon of $\{V_2TeO_8\}_n$ in **1**.

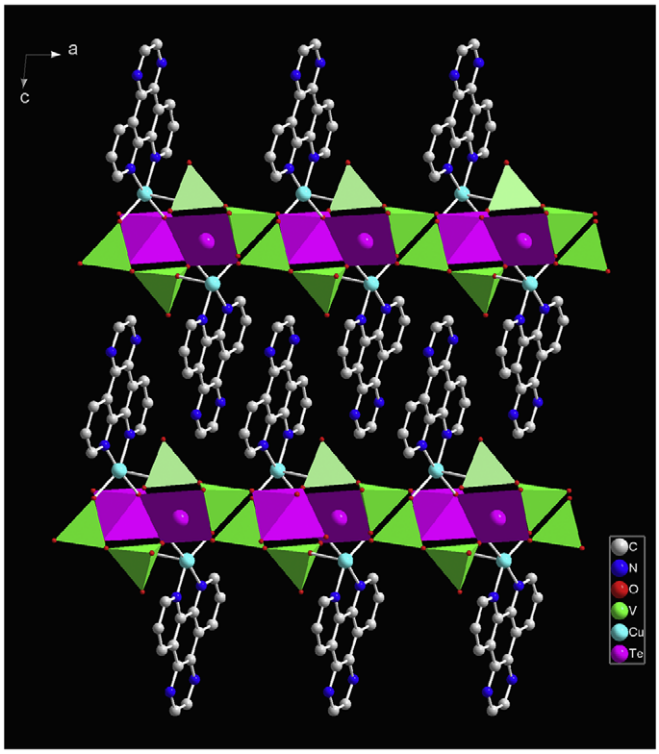

Fig. 4. 3D organic–inorganic supramolecular framework of **1**, showing $\pi-\pi$ stacking interactions.

bridging oxygen atoms, which are linked with one Te(2) atom, one Te(1) atom and one Cu atom individually. It is interesting that there are also two crystallographically distinct tellurite atoms in the asymmetric unit. Te(1) atom is four-coordinate and exhibits an AX4E trigonal bipyramid geometry coordinated with four oxygen atoms. However, Te(2) atom features an unusual coordination environment, which is coordinated with one terminal oxygen atom and two bridging oxygen atoms to form a tetrahedral geometry by taking the lone pair electrons into consideration [22]. The previously reported pure inorganic vanadium tellurite phases $NaVTeO_5$ with the same empirical formula [25] features the $[Te_2O6]$ motifs, consisting of two edge-sharing {TeO4} trigonal bipyramid, interconnect two $\{VO_4\}$ tetrahedron via corner-sharing to form a 1D chain structure.

The most interesting aspect of the structure of **2** is that there exist two kinds of layers, which contains chains of opposite chirality but equivalent conformation and these different chains are thus enantiomorphous. Because these layers, being parallel to the *ac* plane, possess left-handed and right-handed characterization alternately, each layer thus becomes a chiral component. The two types of layers, one left-handed and the other right-handed, pairwise crystallize in a space group $P2_1/c$, leading to a racemic solid-state compound. In left-handed layer, there exist two types of left-handed inorganic helical chains $(V_4Te_4O_8)_n$ and $(Te_2O_2)_n$. Two types of helical chains are linked by μ_3 oxygen atoms (O6) to generate an unexpected chiral V–O–Te inorganic anionic layer (Fig. 2S). However, in the adjacent layer, there also exist two types of helical chains with the reverse handedness (Fig. 6). To the best of our knowledge, two types of homochiral helical chains, Te–O–Te and V–O–Te–O–V–O, in a chiral layer architecture have not been reported although chiral layer architecture has been previously reported [26].

While more studies are needed to clearly elucidate the causes of the chirality and the racemization, our results did provide some evidence for a tentative explanation. A comparison of **1** with **2**

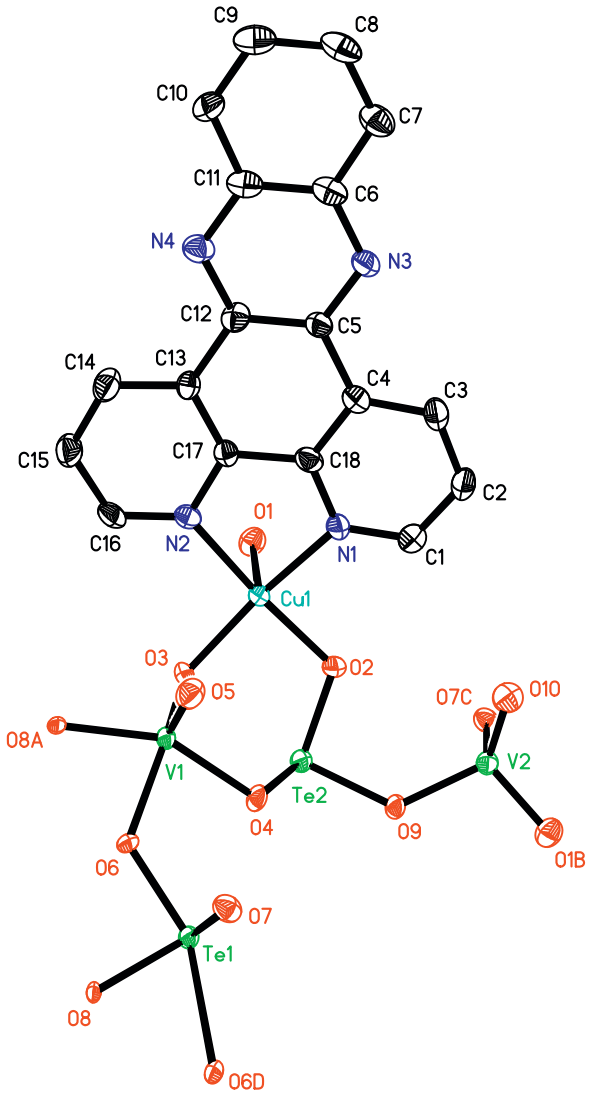

Fig. 5. ORTEP drawing of **2** with thermal ellipsoids at 50% probability. H atoms are omitted for clarity.

suggests that the larger DPPZ ligand may be responsible for the formation of the chiral framework. Although the two compounds have similar composition, with the only difference in employing two different organic ligands (TATP and DPPZ), respectively, compound **2** has an enantiomorphous chiral crystal structure whereas **1** does not. Compared with TATP, the larger aromatic DPPZ ligand could further enhance the $\pi-\pi$ aromatic stacking interactions, which are the possible driving force to induce the formation of the chirality. Similarly, several researches also showed that the size of organic ligand plays an important role in the formation of non-centrosymmetric solids and helical chains [27].

The stacking of sheets manifests considerable overlap of the DPPZ ligands between the adjacent layers with an average interplanar separation of *ca.* 3.55 Å (Fig. 1S). The carbon atoms of DPPZ ligand also have C–H$\cdots\pi$ interactions with an adjacent DPPZ aromatic ring. The distance of C8$\cdots$ring centroid of plane (C1,C2,C3,C4,C18,N1) is 3.376 Å. Obviously, the $\pi-\pi$ and C–H$\cdots\pi$ stacking interactions between the DPPZ groups make the neighboring layers stably packed together [28]. Additionally, the weak intra- and interlayer hydrogen bonding interactions also perform a certain function on stabilizing the chiral layer structure of **2** and the typical hydrogen bonds are C1$\cdots$O10 (x, $y-1$, z)

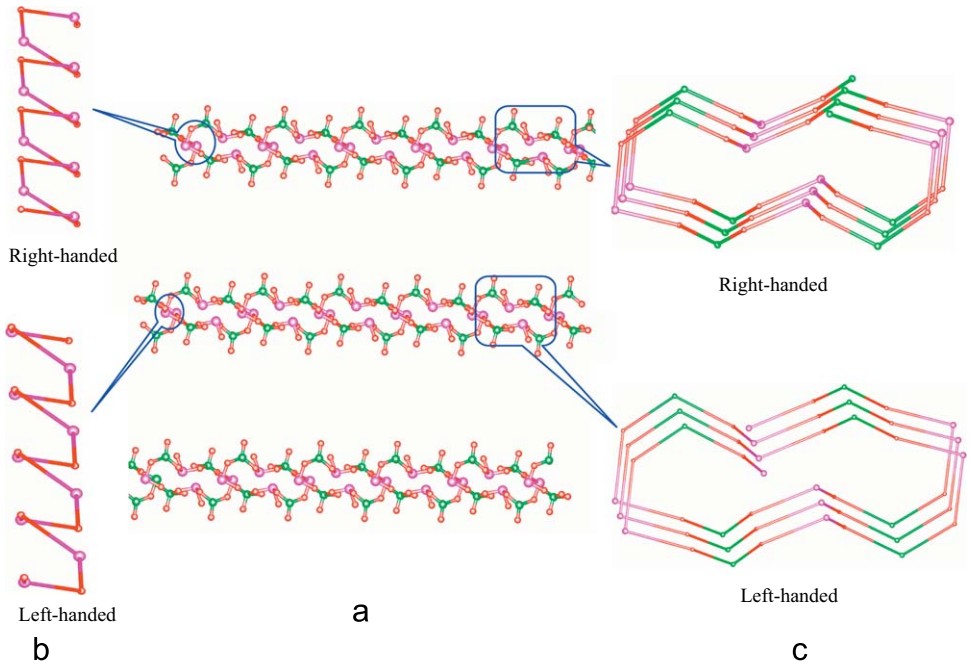

Fig. 6. (a) Representation of the two types of chiral V–O–Te layers in **2** along the *b* axis, one left-handed and another right-handed, respectively. (b) Left-handed and right-handed Te–O–Te helical chains. (c) Left-handed and right-handed $V_4Te_4O_8$ helical chains. Te, purple; V, green; O, red. (For interpretation of the references to color in this figure legend, the reader is referred to the web version of this article.)

3.290(2) Å, C7⋯O10 (−*x*+1, *y*+3/2,−*z*+1/2) 3.362(2) Å, C15⋯O5 (−*x*+1,−*y*,−*z*) 3.431(2) Å.

The bond valence sum calculations [29] indicate that all V atoms are in the +5 oxidation state, the Te atoms are in the +4 oxidation state and the Cu atoms are in the +2 oxidation state in both **1** and **2**.

In the IR spectrum of **1**, 933 and 841 cm^{-1} are due to the terminal *v*(V–O) stretch or a *v*(V–O–V) stretch. Bands at 788, 731, 636 cm^{-1} are assigned to *v*(Te–O), *v*(Te–O–V), *v*(Te–O–Cu). Bands at 1625–1114 cm^{-1} are characteristic of TATP ligand. In the IR spectrum of **2**, vibration bands at 961, 868 cm^{-1} are due to the terminal *v*(V–O) stretch or a *v*(V–O–V) stretch. Bands at 817, 779, 725, 678 cm^{-1} are assigned to *v*(Te–O), *v*(Te–O–V), *v*(Te–O–Cu). Bands at 1623–1139 cm^{-1} are characteristic of DPPZ ligand.

4. Conclusions

In summary, two new organic–inorganic hybrid vanadium tellutites, Cu(TATP)V_2TeO_8 (**1**) and Cu(DPPZ)$V_2Te_2O_{10}$ (**2**), have been synthesized and characterized. Compound **1** contains a new double-chain-like ribbons composed of unexpected eight-membered rings $\{V_4Te_4O_8\}_n$. Compound **2** is a chiral layer architecture with left-handed and right-handed characterization alternately, thus leading to a racemic solid-state compound. In each layer, there exist two types of inorganic helical chains, $(V_4Te_4O_8)_n$ and $(Te_2O_2)_n$, with identical handedness. Interestingly, in the adjacent layer, there also exist two types of helical chains with the reverse handedness. It should be noted that **1** and **2** were synthesized under the same conditions, the only difference in employing two different aromatic chelate ligands (TATP and DPPZ), respectively, compound **2** has an enantiomorphous chiral crystal structure whereas **1** does not, suggesting that the larger DPPZ ligand could further enhance the $\pi-\pi$ aromatic stacking interactions, which are possible driving force to induce the formation of the chirality.

Acknowledgment

This work was granted financial support from National Natural Science Fundation of China (Grant 20871063).

Appendix A. Supplementary data

Supplementary data associated with this article can be found in the online version at doi:10.1016/j.jssc.2009.05.038.

References

[1] C.T. Kressge, M.E. Leonowicz, W.J. Roth, J.C. Vartuni, J.S. Beck, Nature 359 (1992) 710.
[2] [a] C.L. Bowes, G.A. Ozin, Adv. Mater. 8 (1996) 13;
[b] S. Kitagawa, M. Kondo, Bull. Chem. Soc. Jpn. 71 (1998) 1739;
[c] C.R. Kagan, D.B. Mitzi, C.D. Dimitrakopoulos, Science 286 (1999) 945;
[d] P.S. Halasyamani, M.J. Drewitt, D. O'Hare, Chem. Commun. (1997) 867.
[3] P.M. Forster, A.K. Cheetham, Angew. Chem. Int. Ed. Engl. 41 (2002) 457.
[4] J. Tao, X.M. Zhang, M.L. Tong, X.M. Chen, J. Chem. Soc. Dalton Trans. (2001) 770.
[5] L. Xu, M. Lu, B.B. Xu, Y.G. Wei, Z.H. Peng, D.R. Powell, Angew. Chem. Int. Ed. Engl. 41 (2002) 4129.
[6] [a] P.J. Hagrman, D. Hagrman, J. Zubieta, Angew. Chem. Int. Ed. Engl. 38 (1999) 2638;
[b] P.J. Hagrman, J. Zubieta, Inorg. Chem. 39 (2000) 3252;
[c] P.J. Hagrman, J. Zubieta, Inorg. Chem. 40 (2001) 2800;
[d] P.J. Hagrman, R.C. Finn, J. Zubieta, Solid State Sci. 3 (2001) 745.
[7] C.M. Liu, Y.L. Hou, J. Zhang, S. Gao, Inorg. Chem. 41 (2002) 140.
[8] [a] C.W. Hu, Q.L. He, Y.H. Zhang, Y.Y. Liu, Y.F. Zhang, T.D. Tang, J.Y. Zhang, E.B. Wang, Chem. Commun. (1996) 121;
[b] L.H. Bi, E.B. Wang, J. Peng, L. Xu, C.W. Hu, Inorg. Chem. 39 (2000) 671;
[c] L. Xu, Y.Q. Sun, E.B. Wang, E.H. Shen, Z.R. Liu, C.W. Hu, Y. Xing, Y.H. Lin, H.Q. Jia, New J. Chem. 23 (1999) 1041;
[d] M. Yuan, Y.G. Li, E.B. Wang, Y. Lu, C.W. Hu, N.H. Hu, H.Q. Jia, J. Chem. Soc. Dalton Trans. (2002) 2916;
[e] Y. Lu, E.B. Wang, M. Yuan, G.Y. Luan, Y.G. Li, J. Chem. Soc. Dalton Trans. (2002) 3029;
[f] G.Y. Luan, Y.G. Li, S.T. Wang, E.B. Wang, Z.B. Han, C.W. Hu, N.H. Hu, H.Q. Jia, Dalton Trans. (2003) 233;

[g] Y.G. Li, G.J.H. De, M. Yuan, E.B. Wang, R.D. Huang, C.W. Hu, N.H. Hu, H.Q. Jia, Dalton Trans. (2003) 331;
[h] Y.M. Chen, E.B. Wang, B.Z. Lin, S.T. Wang, J. Chem. Soc. Dalton Trans. (2003) 519.
[9] [a] X.M. Zhang, M.L. Tong, S.H. Feng, X.M. Chen, J. Chem. Soc. Dalton Trans. (2001) 2069;
[b] X.M. Zhang, M.L. Tong, X.M. Chen, Chem. Commun. (2000) 1817.
[10] [a] C.M. Liu, S. Gao, H.M. Hu, Z.M. Wang, Chem. Commun. (2001) 1636;
[b] C.M. Liu, S. Gao, H.Z. Kou, Chem. Commun. (2001) 1670.
[11] [a] L.R. Zhang, Z. Shi, G.Y. Yang, X.M. Chen, S.H. Feng, J. Chem. Soc. Dalton Trans. (2000) 275;
[b] Z. Shi, S.H. Feng, S. Gao, L. Zhang, G.Y. Yang, J. Hua, Angew. Chem. Int. Ed. Engl. 39 (2000) 2325.
[12] [a] L.H. Huang, H.M. Kao, K.H. Lii, Inorg. Chem. 41 (2002) 2936;
[b] L.M. Zheng, J.S. Zhao, K.H. Lii, L.Y. Zhang, Y. Liu, X.Q. Xin, J. Chem. Soc. Dalton Trans. (1999) 939.
[13] [a] D.R. Xiao, Y.G. Li, E.B. Wang, S.T. Wang, Y. Hou, G.J.H. De, C.W. Hu, Inorg. Chem. 42 (2003) 7652;
[b] J.Y. Xie, J.G. Mao, Inorg. Chem. Commun. 8 (2005) 375;
[c] M.L. Feng, J.G. Mao, J. Solid State Chem. 178 (2005) 2256.
[14] S. Banfi, L. Carlucci, E. Caruso, G. Ciani, D.M. Proserpio, J. Chem. Soc. Dalton Trans. (2002) 2714.
[15] [a] R. Robson, B.F. Abrahams, S.R. Batten, R.W. Gable, B.F. Hoskins, J. Lieu, in: T. Bein (Ed.), Supramolecular Architecture, ACS, Washington, DC, 1992, p. 256;
[b] D.L. Long, A.J. Blake, N.R. Champness, C. Wilson, M. Schröder, Chem. Eur. J. 8 (2002) 2027;
[c] S. Subramanian, M.J. Zaworotko, Angew. Chem. Int. Ed. Engl. 34 (1995) 2127;
[d] R.W. Gable, B.F. Hoskins, R. Robson, Chem. Commun. (1990) 1677.
[16] [a] M.L. Tong, X.M. Chen, B.H. Ye, S.W. Ng, Inorg. Chem. 37 (1998) 2645;
[b] C.Y. Su, Y.P. Cai, C.L. Chen, F. Lissner, B.S. Kang, W. Kaim, Angew. Chem. Int. Ed. Engl. 41 (2002) 3371;
[c] T.L. Honnigar, D.C. MacQuarric, P.D. Rogers, M.J. Zaworotko, Angew. Chem. Int. Ed. Engl. 36 (1997) 972;
[d] H. Gudbjarlson, K.M. Poirier, M.J. Zaworotko, J. Am. Chem. Soc. 121 (1999) 2599.
[17] [a] L. Carlucci, G. Ciani, D.M. Proserpio, Angew. Chem. Int. Ed. Engl. 34 (1995) 1895;
[b] M.L. Tong, X.M. Chen, B.H. Ye, S.W. Ng, Inorg. Chem. 37 (1998) 5168;
[c] A.J. Blake, N.R. Champness, P. Hubberstey, W.S. Li, M.A. Withersby, M. Schröder, Coord. Chem. Rev. 183 (1999) 117;
[d] H.L. Zhu, Y.X. Tong, X.M. Chen, J. Chem. Soc. Dalton Trans. (2000) 4182.
[18] [a] R.Q. Zou, J.R. Li, Y.B. Xie, R.H. Zhang, X.H. Bu, Cryst. Growth Des. 4 (2004) 79;
[b] J.R. Li, R.H. Zhang, X.H. Bu, Cryst. Growth Des. 3 (2003) 829;
[c] C.L. Chen, C.Y. Su, Y.P. Cai, H.X. Zhang, A.W. Xu, B.S. Kang, H.C. zur Loye, Inorg. Chem. 42 (2003) 3738.
[19] [a] Z.B. Han, X.N. Cheng, X.M. Chen, Cryst. Growth Des. 2 (2005) 695;
[b] Y.Z. Zheng, G.F. Liu, B.H. Ye, X.M. Chen, Z. Anorg. Allg. Chem. 630 (2004) 296.
[20] [a] J.G. Collins, A.D. Sleeman, J.R. Aldrich-Wright, I. Greguric, T.W. Hambley, Inorg. Chem. 37 (1998) 3133;
[b] J.E. Dickeson, L.A. Summers, Aust. J. Chem. 23 (1970) 1023.
[21] SHELXTL 6.10, Bruker Analytical Instrumentation, Madison, Wisconsin, USA, 2000.
[22] M.G. Johnston, W.T.A. Harrison, J. Am. Chem. Soc. 124 (2002) 4576.
[23] [a] Z.B. Han, Y.K. He, C.H. Ge, J. Ribas, L. Xu, Dalton. Trans. (2007) 3020;
[b] M.L. Tong, H.J. Chen, X.M. Chen, Inorg. Chem. 39 (2000) 2235;
[c] C. Janiak, J. Chem. Soc. Dalton Trans. (2000) 3885.
[24] K. Sugiura, Y. Sakata, T. Tanaka, M. Sawada, Chem. Lett. (1997) 281.
[25] J. Darriet, G. Guillaume, K.-A. Wilhelmi, J. Galy, Acta Chem. Scand. 26 (1972) 59.
[26] C. Qin, L. Xu, Y.G. Wei, X.L. Wang, F.Y. Li, Inorg. Chem. 42 (2003) 3107.
[27] [a] X.M. Chen, G.F. Liu, Chem. Eur. J. 8 (2002) 4811;
[b] P.A. Maggard, C.L. Stern, K.R. Poeppelmeier, J. Am. Chem. Soc. 123 (2001) 7742.
[28] Z.B. Han, Y. Ma, Z.G. Sun, W.S. You, Inorg. Chem. Commun. 9 (2006) 844.
[29] D. Brown, D. Altermatt, Acta Crystallogr. Sect. B 41 (1985) 244.